Available online at www.sciencedirect.com
ScienceDirect
Journal of Sound and Vibration 305 (2007) 151–171
JOURNAL OF SOUND AND VIBRATION
www.elsevier.com/locate/jsvi

A novel way to detect transverse surface crack in a rotating shaft

Ashish K. Darpe

Department of Mechanical Engineering, Indian Institute of Technology Delhi, Hauz Khas, New Delhi-110016, India

Received 8 January 2007; accepted 22 March 2007
Available online 30 May 2007

Abstract

This paper presents a novel way to detect fatigue transverse cracks in rotating shafts. The proposed detection methodology exploits both the typical nonlinear breathing phenomenon of the crack and the coupling of bending–torsional vibrations due to the presence of crack for its diagnosis. A transient torsional excitation is applied for a very short duration at specific angular orientation of the rotor and its effect in the lateral vibrations is investigated. Wavelet transforms (WTs) is used in revealing the transient features of the resonant bending vibrations, which are set up for a short duration of time upon transient torsional excitation. Variation of peak absolute value of wavelet coefficient (of the transient lateral vibration response) with angle at which torsional excitation is applied is investigated. The correlation of this variation with the breathing pattern of the crack is studied. The sensitivity of the proposed methodology to the depth of crack is investigated. The detection methodology gives a vibration response signature that closely correlates with and is very specific to the behaviour of the transverse surface crack in a horizontal rotor. The response features are not likely to be exhibited by other common rotor faults under similar excitation conditions making the proposed detection methodology unambiguous. The fact that the rotor is not required to stop and that the detection process is applied for a rotating shaft with only a short period transient external excitation makes the methodology more convenient.

1. Introduction

Fatigue cracks are a potential source of catastrophic failures in rotors. Researchers have put in considerable effort to develop a foolproof and reliable strategy to detect cracks in rotors. One of the approaches investigated in detail is the phase and amplitude variation in the $2x$ component of steady-state (unbalance) response. Due to the asymmetry of the stiffness due to the existence of crack, several authors [1–7] have focused their attention on $1x$ and $2x$ components of rotor vibration and discussed the effect of crack on these frequency components. Experience, however, has shown that even for shallow to moderate cracks, the presence of $2x$ component of vibration cannot be considered as a reliable indicator of the presence of a crack in the rotor since there are several other mechanisms in rotor that generate second harmonic ($2x$) component. Although the crack breathing is responsible for the presence of higher harmonic component ($3x$) in the response, its amplitude is very small. The presence of higher harmonics cannot conclusively single out the crack as a fault in the rotor as there are several other mechanisms in the rotor bearing system that generate the higher harmonics.

E-mail address: akdarpe@mech.iitd.ernet.in.

0022-460X/$ - see front matter © 2007 Elsevier Ltd. All rights reserved.
doi:10.1016/j.jsv.2007.03.070

Nomenclature

a	depth of crack
R, D	radius and diameter of the shaft, respectively
A	cross-sectional area
$\bar{a}$	crack depth ratio (a/D) for crack
b	half-width of the crack
l	length of the shaft element containing crack
x	location of crack in the finite element
m_d	mass of the disc
h	height of the elemental strip
I	area moment of inertia for the cross section
E	Young's modulus
G	modulus of rigidity
P_i	nodal forces on the crack element
K_{Ij}	stress intensity factor in Ith mode due to load in jth direction
K^o	overall stress intensity factor contributing to opening mode
t	time in seconds
M_t	magnitude of torsional excitation
$[M]^s, [C]^s, [K]^s$	mass, damping and stiffness matrix of the rotor system in stationary coordinate system
$[K]^r$	stiffness matrix of the rotor system in rotating coordinate system
k_{ij}	element of the rotor system stiffness matrix
$\{q\}^s$	rotor response in stationary coordinate system
$\{q\}^r$	rotor response in rotating coordinate system
$\{f\}^s$	forces on the rotor in stationary coordinate system
$[T]$	transformation matrix for the finite element
$[G_f]$	flexibility matrix of the crack element
$[K]^c$	stiffness matrix of the crack finite element
$C_{a,b}$	wavelet coefficient

Greek symbols

α	crack depth for the elemental strip
α_s	shear coefficient of the cross section
β	location of elemental strip along y direction
ε	eccentricity of mass of disc from its geometric centre
φ	angle of rotation of shaft
φ_c	cumulative angle of rotation of shaft (total angle turned)
ω	rotational speed in rad/s

Alternative to the detection of cracks using higher harmonic components in bending vibration, another detection methodology explored the effect of coupling between lateral, axial and torsional vibrations caused by the presence of crack in a rotor. Papadopoulos and Dimarogonas [8,9] first proposed this effect as a useful and more reliable source for the detection of cracks. The presence of bending vibration frequencies in torsional spectra had been cited as potential crack indicators. Muszynska et al. [10] analysed torsional/lateral cross-coupled vibration response. Ostachowicz and Krawczuk [11] analysed coupled torsional and bending vibrations of a rotor with an open crack using finite element model. They applied an external torsional moment to the rotor and found the effect on lateral vibrations due to coupling effect of crack. Papadopoulos and Dimarogonas [12] studied coupling of lateral and longitudinal vibrations and have proposed the coexistence of lateral and longitudinal vibration frequencies in the same spectrum as an unambiguous crack indicator. Papadopoulos and Dimarogonas [13] have studied the stability of cracked shaft in coupled vibration mode. The effect of closing crack was taken into account by representing variation in stiffness in the form of a truncated cosine series. A case study on 300 MW steam turbine, wherein the lateral vibration spectrum showed subharmonics of fundamental longitudinal natural frequency was reported. Darpe et al. [14,15] and Collins et al. [16] studied the detection of cracks using axial impulses to a rotating cracked shaft. They reported the presence of combination harmonics in the lateral vibration spectrum. Gounaris and Papadopoulos [17] investigated coupled vibration response between bending and longitudinal vibration by applying lateral excitation and measuring longitudinal vibrations on a rotating shaft with open crack assumptions.

Although [14–16] were perhaps the only studies on coupled vibrations of cracked rotors with breathing crack model, most of the previous reported work focused on open crack model. The open crack

model in early studies served the purpose of reducing the stiffness of the rotor to account for the effect of the crack. However, to represent the actual breathing behaviour of the cracked rotor, change in the stiffness due to rotation of the rotor under gravity must be appropriately modelled. The crack breathing is a significant source of several nonlinear phenomena that cannot be revealed through the open crack model. Recently, this fact has been explored extensively by Darpe et al. [18]. They studied the effect of using exact breathing model for rotating shaft and investigated the coupling between all modes of vibration for cracked rotor. They proposed several new crack indicators and showed that these indicators are sensitive to crack depth.

Using Alternate Frequency/Time Domain (AFT) and path following method, Sinou and Lees investigated the change of natural frequencies, harmonic components and evolution of orbital pattern of the cracked rotor at half the critical speed [19]. Recently, model-based identification of crack has also been attempted [20,21].

In the recent past several researchers have applied the wavelet transforms (WTs) for analysis of dynamic signals of the variety of mechanical systems to detect faults such as crack, bearing defects, rotor rub, etc. Adewusi and Al-Bedoor [22] applied WT to experimental signal of propagating transverse crack to track the growth of important harmonic components of the rotor speed. Zou and Chen [23] made a comparative study on time–frequency feature of transient response of cracked rotor by Wigner–Ville distribution and WT. Wan et al. [24] carried out vibration analysis of cracked rotor sliding bearing system with rotor-stator rubbing by harmonic WT. Zou et al. [25] analysed the torsional vibrations of a rotor with transverse crack using switching crack model and time–frequency features of torsional vibrations of the rotor are presented using WT. Prabhakar et al. [26] investigated the use of continuous wavelet transforms (CWTs) for crack detection and monitoring in a cracked rotor system during its transient passage through critical speed. In none of the above studies on application of WT to crack detection, an unambiguous detection strategy of crack with certainty could be proposed. The major problem, of distinguishing the cracked rotor response from that of the nonlinear response generated by other similar faults, still remains unsolved.

In this paper, the breathing crack model is used to investigate a novel use of transient external torsional excitation for crack detection. The torsional excitation is applied at specific angular position of the rotating shaft so that the periodic opening and closing of the crack is exploited to generate distinguishing response characteristics that is typical to the cracked rotor and cannot be expected in case of other rotor faults. The proposed crack detection strategy uses the coupling of vibrations of cracked rotor and breathing behaviour of crack. The proposed detection strategy is more reliable and unambiguous.

In this work, finite element model of a simple single disc rotor is considered. The rotor is modelled with Timoshenko beam elements and a rotor segment containing a transverse surface crack at centre of the span is modelled with a Timoshenko beam element with modified stiffness matrix derived in Ref. [18]. The modified stiffness matrix takes into account all the coupling phenomena that exists in a cracked rotor, i.e., bending-longitudinal, bending-torsion, longitudinal-torsion. The FE model of the rotor with six degrees of freedom per node and modified stiffness matrix for cracked region is used to study lateral vibration response of the rotor subjected to transient torsional excitation.

2. Finite element model and breathing behaviour of the cracked rotor

A rotor bearing system as shown in Fig. 1c is modelled as an assemblage of 14 finite elements of which one element is a modified Timoshenko Beam element while the others are standard Timoshenko beam element. Consider a rotor segment containing a single transverse surface crack. A beam finite element containing a transverse surface crack of depth a as shown in Fig. 1. The modified stiffness matrix for Timoshenko beam element accounting for the additional strain energy due to the presence of crack is derived in Ref. [18] and is given as

$$[K]^c = [T][G_f]^{-1}[T]^{\mathrm{T}}, \tag{1}$$

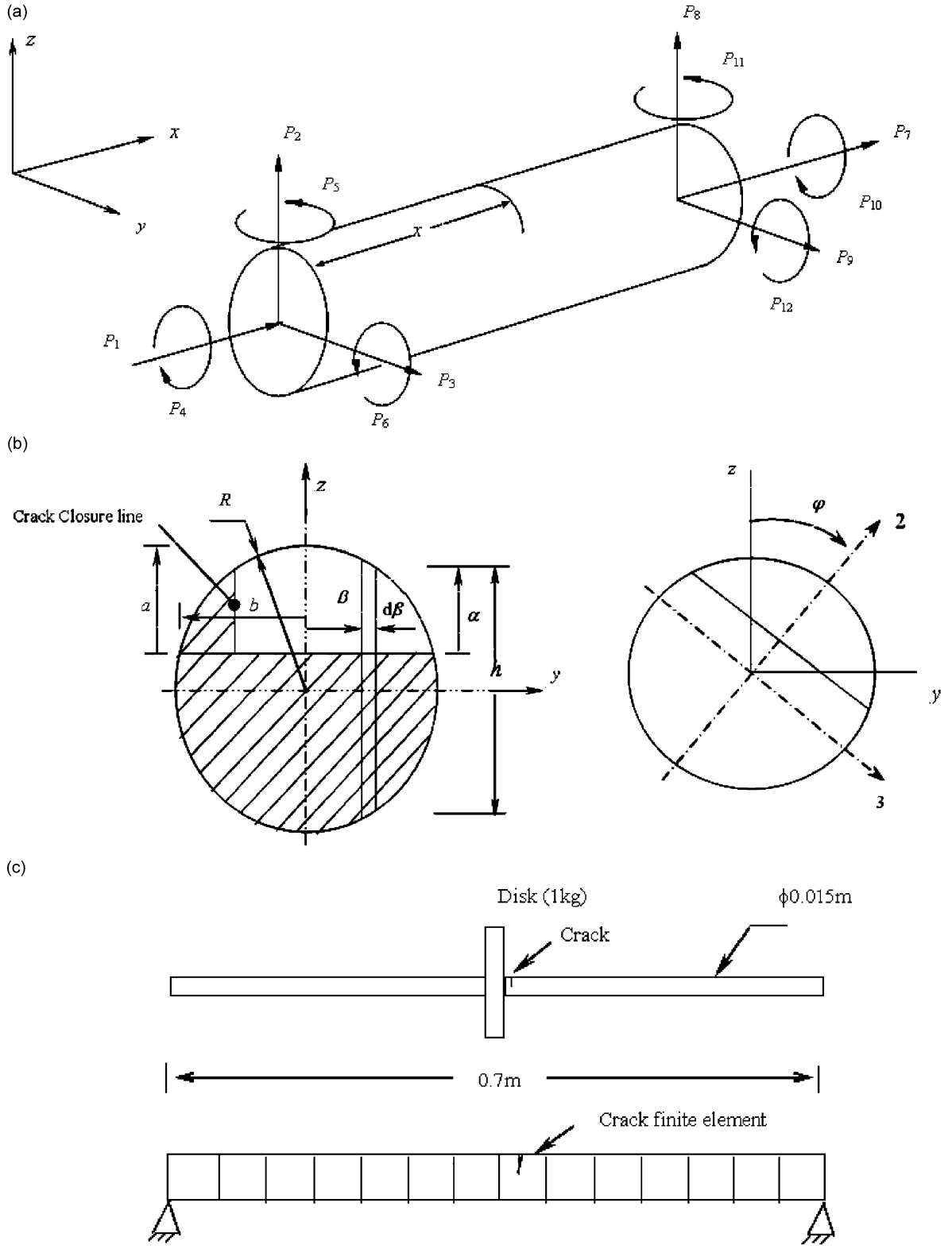

Fig. 1. Shaft finite element: (a) the element showing forces acting and coordinate system; (b) crack cross section; (c) a simple rotor and its finite element model.

where the transformation matrix $[T]$ is given by

$$[T]^{\mathrm{T}} = \begin{bmatrix} 1 & 0 & 0 & 0 & 0 & 0 & -1 & 0 & 0 & 0 & 0 & 0 \\ 0 & 1 & 0 & 0 & 0 & 0 & 0 & -1 & 0 & 0 & 0 & l \\ 0 & 0 & 1 & 0 & 0 & 0 & 0 & 0 & -1 & 0 & -l & 0 \\ 0 & 0 & 0 & 1 & 0 & 0 & 0 & 0 & 0 & -1 & 0 & 0 \\ 0 & 0 & 0 & 0 & 1 & 0 & 0 & 0 & 0 & 0 & -1 & 0 \\ 0 & 0 & 0 & 0 & 0 & 1 & 0 & 0 & 0 & 0 & 0 & -1 \end{bmatrix}$$

and the flexibility matrix $[G_f]$ for the crack element is given by

$$G_f = \begin{bmatrix} g_{11} & g_{12} & g_{13} & g_{14} & g_{15} & g_{16} \\ g_{21} & g_{22} & g_{23} & g_{24} & g_{25} & g_{26} \\ g_{31} & g_{32} & g_{33} & g_{34} & g_{35} & g_{36} \\ g_{41} & g_{42} & g_{43} & g_{44} & g_{45} & g_{46} \\ g_{51} & g_{52} & g_{53} & g_{54} & g_{55} & g_{56} \\ g_{61} & g_{62} & g_{63} & g_{64} & g_{65} & g_{66} \end{bmatrix}. \tag{2}$$

In the above matrix, the flexibility coefficients are as under [18]

$$g_{11} = \frac{l}{AE} + \int_A \frac{2\alpha F_1^2}{\pi E R^4}\,\mathrm{d}A, \quad g_{22} = \left(\frac{\alpha_s l}{GA} + \frac{l^3}{3EI}\right) + \int_A \left(\frac{2k^2\alpha F_{\mathrm{II}}^2}{\pi E R^4} + \frac{8x^2h^2\alpha F_2^2}{\pi E R^8}\right)\mathrm{d}A,$$

$$g_{33} = \left(\frac{\alpha_s l}{GA} + \frac{l^3}{3EI}\right) + \int_A \left(\frac{2mk^2\alpha F_{\mathrm{III}}^2}{\pi E R^4} + \frac{32x^2\beta^2\alpha F_1^2}{\pi E R^8}\right)\mathrm{d}A,$$

$$g_{44} = \frac{l}{GI_0} + \int_A \left(\frac{8\beta^2\alpha F_{\mathrm{II}}^2}{\pi E R^8} + \frac{2mh^2\alpha F_{\mathrm{III}}^2}{\pi E R^8}\right)\mathrm{d}A, \quad g_{55} = \frac{l}{EI} + \int_A \frac{32\beta^2\alpha F_1^2}{\pi E R^8}\,\mathrm{d}A,$$

$$g_{66} = \frac{l}{EI} + \int_A \frac{8h^2\alpha F_2^2}{\pi E R^8}\,\mathrm{d}A, \quad g_{12} = g_{21} = \int_A \frac{4xh\alpha F_1 F_2}{\pi E R^6}\,\mathrm{d}A, \quad g_{13} = g_{31} = \int_A \frac{8x\beta\alpha F_1^2}{\pi E R^6}\,\mathrm{d}A,$$

$$g_{15} = g_{51} = \int_A \frac{8\beta\alpha F_1^2}{\pi E R^6}\,\mathrm{d}A, \quad g_{16} = g_{61} = -\int_A \frac{4h\alpha F_1 F_2}{\pi E R^6}\,\mathrm{d}A, \quad g_{23} = g_{32} = \int_A \frac{16x^2h\beta\alpha F_1 F_2}{\pi E R^8}\,\mathrm{d}A,$$

$$g_{24} = g_{42} = \int_A \frac{4k\alpha\beta F_{\mathrm{II}}^2}{\pi E R^6}\,\mathrm{d}A, \quad g_{34} = g_{43} = \int_A \frac{2mkh\alpha F_{\mathrm{III}}^2}{\pi E R^6}\,\mathrm{d}A, \quad g_{25} = g_{52} = \int_A \frac{16xh\beta\alpha F_1 F_2}{\pi E R^8}\,\mathrm{d}A,$$

$$g_{35} = g_{53} = \frac{l^2}{2EI} + \int_A \frac{32x\beta^2\alpha F_1^2}{\pi E R^8}\,\mathrm{d}A, \quad g_{26} = g_{62} = -\frac{l^2}{2EI} - \int_A \frac{8xh^2\alpha F_2^2}{\pi E R^8}\,\mathrm{d}A,$$

$$g_{36} = g_{63} = -\int_A \frac{16xh\beta\alpha F_1 F_2}{\pi E R^8}\,\mathrm{d}A, \quad g_{56} = g_{65} = -\int_A \frac{16h\beta\alpha F_1 F_2}{\pi E R^8}\,\mathrm{d}A. \tag{3}$$

In above equation, $m = 1 + \nu$, where ν is Poisson's ratio and F_1, F_2 and F_{III} are functions as defined in Ref. [18]. Some flexibility coefficients such as g_{14}, g_{41}, g_{45}, etc. are zero [18].

When the rotor is operating at a steady-state speed far away from critical speed and without any transient excitation, the breathing of the crack can be approximated either by sinusoidal stiffness variation or by stepwise stiffness fluctuation. However, a truly breathing behaviour can be represented by taking into account the gradual opening and closing of the crack using the sign of stress intensity factor at the crack edge at each instant and then finding the amount of crack opening and hence the stiffness. In this way, apart from getting

a more accurate estimation of stiffness and more realistic representation of breathing, the model would be adaptable for all speed ranges and all type of excitations, steady as well as transient.

For accounting for the breathing of crack, the stress intensity factor (SIF) at all locations on the crack edge is estimated. SIF is a measure of the stress-field intensity (stress state) near the tip of an ideal crack in a linear-elastic solid when the crack surfaces are displaced in standard mode of displacement. The negative SIF at any position along the crack edge indicates compressive stress and hence a closed state of crack; while the positive SIF indicates tensile stress and open state of crack. Once the open and closed portion of crack edge is estimated, the integration limits for the evaluation of the flexibility coefficients using Eq. (3) are decided (the integration limit for crack width must be for the open length of crack edge). The integration limits decides the value of flexibility coefficient and hence the stiffness value.

The calculation of stiffness of cracked element and the response estimation are interdependent. This is because the response is dependent on the stiffness values used in the equation of motion and stiffness values are estimated from the rotor response using the sign of SIF values as elaborated in following paragraphs. The equation of motion for the rotor bearing system in stationary coordinates is

$$[M]^s\{\ddot{q}\}^s + [C]^s\{\dot{q}\}^s + [K]^s\{q\}^s = \{f\}^s, \tag{4}$$

where, $[M]^s$, $[C]^s$ and $[K]^s$ are mass, damping and stiffness matrices for the rotor system in stationary coordinate system. Of these, only stiffness matrix is constantly updated, usually after every degree of rotation, as it is assumed response dependent. The mass and damping matrices are assumed constant. Proportional damping matrix is assumed here with $[C]^s = \alpha_d[K_{uc}] + \beta_d[M]$, where the constants α_d and β_d are assumed equal to 0.8132 and 1.3623e−5, respectively. These constants are evaluated based on the assumption of modal damping ratios of 0.005 and 0.01 in the first two modes of the uncracked rotor system. $[K_{uc}]$ is the stiffness matrix without crack. The force vector $\{f\}^s$ contains gravity and unbalance excitation forces. When applied, torsional excitation terms also appear in the force vector.

The solution scheme for the estimation of response of the cracked rotor is as follows. Using an initial assumed response vector $\{q\}^s$ and stiffness matrix $[K]^s$, Eq. (4) is integrated following the Newmark method of direct numerical integration. The integration parameters $\alpha_i = 0.25$ and $\delta_i = 0.5$ are used to estimate the response of the rotor. The integration time step Δt is assumed to be 1/50th of the time required for a degree of rotation, which even for a slow speed of 22 rad/s is sufficiently small (1.5867e−5 s). Finer time step has not shown any influence on the response. The integration is carried out for time equal to a degree of rotation during which stiffness matrix in rotor fixed coordinate is assumed constant. Even when the stiffness is changed after every 1/5th of a degree of rotation the resultant response is found to be the same. After each degree of rotation the new response vector $\{q\}^s$ obtained from the integration of Eq. (4) is used to find the response in rotor fixed coordinates $\{q\}^r$ using appropriate coordinate transformation. The nodal forces $[P]$ are then calculated as

$$[P] = [K]^r\{q\}^r. \tag{5}$$

The nodal forces are used to evaluate SIFs as follows [18]:

$$K_{I1} = \frac{P_1}{\pi R^2}\sqrt{\pi\alpha}F_1(\alpha/h), \quad K_{I5} = \frac{4(P_5 + P_3 x)\beta}{\pi R^4}\sqrt{\pi\alpha}F_1(\alpha/h), \quad K_{I6} = \frac{2(P_2 x - P_6)h}{\pi R^4}\sqrt{\pi\alpha}F_2(\alpha/h), \tag{6}$$

where, P_i ($i = 1$–6) are nodal forces as shown in Fig. 1 and the functions F_1 and F_2 are given by

$$F_1 = \sqrt{\frac{2\alpha'}{\pi\alpha}\tan\left(\frac{\pi\alpha}{2\alpha'}\right)}\,\frac{0.752 + 2.02(\alpha/\alpha') + 0.37[1 - \sin(\pi\alpha/2\alpha')]^3}{\cos(\pi\alpha/2\alpha')},$$

$$F_2 = \sqrt{\frac{2\alpha'}{\pi\alpha}\tan\left(\frac{\pi\alpha}{2\alpha'}\right)}\,\frac{0.923 + 0.199[1 - \sin(\pi\alpha/2\alpha')]^4}{\cos(\pi\alpha/2\alpha')}.$$

Overall value of SIF (K^0) at 50 equally spaced points along the crack edge is evaluated using the following relation:

$$K^0 = K_{I1} + K_{I5} + K_{I6}. \tag{7}$$

The SIFs K_{I1}, K_{I5} and K_{I6} only are accounted for in Eq. (7) as they are responsible for opening mode crack displacement. The position along the crack edge where SIF changes its sign is the location of line dividing open and closed area of crack and indirectly indicates the integration limits for Eq. (3). As mentioned earlier, Eq. (3) is to be integrated only for the open area of crack. It may also be noted that the response $\{q\}$ estimated using integration of Eq. (4) decide the nodal forces (through Eq. (5)) and hence the values of SIFs given by Eq. (6). The sign of SIFs in turn decide integration limits for flexibility expressions (Eq. (3)) and hence stiffness of the rotor; the value of stiffness decides the response of the rotor. Thus the rotor response and rotor stiffness in the equations of motion are interdependent.

3. Response of the cracked rotor to transient torsional excitation

To study the coupled bending–torsional vibrations of a cracked rotor, a simply supported rotor with a single centrally situated disc of mass 1 kg is considered. A single transverse surface crack is assumed just adjacent to the central disc. The total rotor span is divided into 14 elements of equal length (Fig. 1c). A crack element that has stiffness properties as described in Section 2, is used to represent the crack. Rest of the rotor is modelled with Timoshenko beam elements with six degrees of freedom per node [27]. To start with, unbalance response of an uncracked rotor with and without torsional excitation is estimated. The response is then compared with that of a cracked rotor. The distinguishing features of the response of cracked rotor from the point of view of crack diagnosis are discussed. Since the breathing of crack causes a continuous response dependent change in the stiffness matrix of the crack element, the Newmark method of direct numerical integration is used to estimate the response. The unbalance eccentricity of 1.6e−5 m is assumed. The rotor rotates at 22 rad/s, which is approximately 1/10th of bending critical speed.

The response as well as the stiffness data for the cracked rotor is stored at every degree of rotation. Fig. 2 shows the variation of direct stiffness for the rotor during a rotation. It shows a reduction of the stiffness of the rotor as the cracked area opens and closes. However, the crack is largely closed from $\varphi = -40^\circ$ (i.e., $\varphi = 320^\circ$) to $\varphi = 40^\circ$ and is open from $\varphi = 140^\circ$ to 220°. Thus, the change in stiffness is not continuous but nonlinear.

Fig. 3 shows the variation of cross-coupled stiffness coefficients relevant for the study of coupled torsional and lateral vibration for the cracked rotor. It may be noted that during the period when the crack is open ($\varphi = 140$–220°) the cross-coupled stiffness involving coupling of torsional mode and shear in direction 2 (k_{24}) is zero whereas the other cross-coupled stiffness involving coupling of torsional mode and shear in direction 3 (k_{34}) is maximum. It shows that when the crack is fully open the torsion is coupled to the shear in direction 3 but not coupled to the shear in direction 2. The value of the cross-coupled stiffness k_{24} is maximum when the crack is half-closed–half-open ($\varphi \approx 90^\circ$) and is zero when fully open ($\varphi \approx 180^\circ$) or fully closed ($\varphi \approx 0^\circ$). Also the variation of cross-coupled stiffness k_{35} and k_{26} indicates that the shear deflections in direction 2 and 3 are coupled to the bending mode deflection (direction 5 and 6, respectively). Although the torsion and bending are not directly coupled, the torsion is coupled to shear in the cracked rotor and the shear in turn is coupled to the bending in the Timoshenko beam element. The torsion–shear coupling exists due to the crack; whereas the shear–bending coupling exists even without the crack. Breathing of the crack only fluctuate the mean value of the cross-coupled stiffness k_{26} (from 51110 to 49850) and k_{35} (from −51110 to −49830) as observed in the figure. Thus unless the crack exists in the rotor, the torsion does not get coupled to the bending vibration. When the crack is partially open, i.e., say from $\varphi = 40^\circ$ to 140° and from $\varphi = 220^\circ$ to 320°, both k_{35} and k_{26} being non-zero, the torsion is coupled to bending. When the crack is fully open the torsion is coupled to shear only in direction 3 and in turn to the bending in direction 5. When the crack is fully closed ($\varphi = 320$–360° and $\varphi = 0$–40°) there is no coupling between torsion and bending as both k_{34} and k_{24} are zero.

The fact that the coupling exists only partly during the rotation of the cracked shaft is the central idea behind the timing of the transient torsional exciation applied to the cracked shaft. It has already been established that when the torsional harmonic excitation is applied, due to the coupling of vibration in case of cracked shaft, the bending vibration spectrum exhibits the presence of torsional excitation frequency [18]. However, sustained harmonic torsional excitation as used in Ref. [18] is required that may not always be

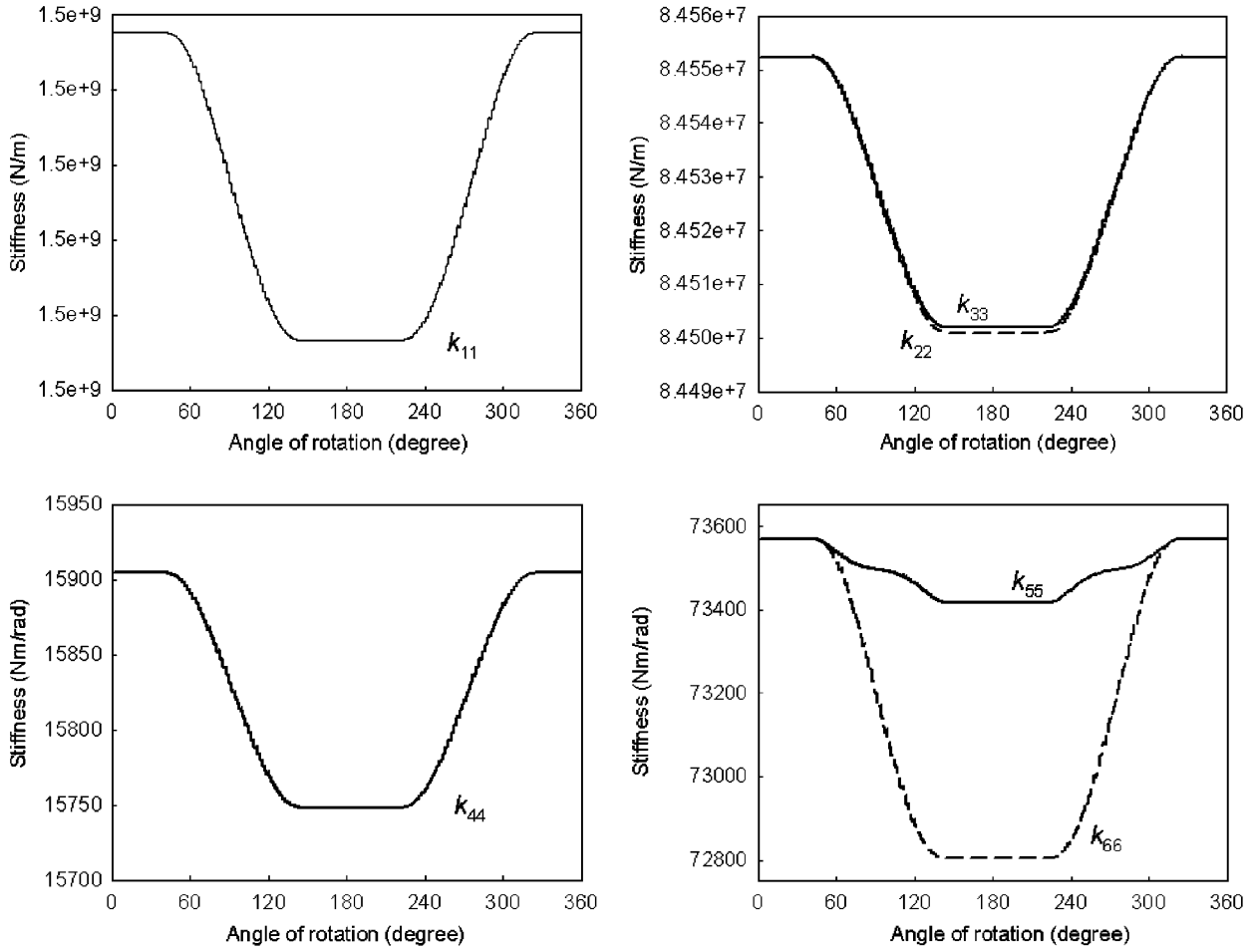

Fig. 2. Variation of direct stiffness coefficients for the cracked rotor ($\bar{a} = 0.2$).

desirable in practice. In the present work, the torsional excitation is applied to a rotating shaft for only a short duration. By applying it when the crack is open and then when it is closed, the response in the two cases is expected to be different because of the presence or absence of the coupling mechanism.

Fig. 4 shows the unbalance response (without torsional excitation) of the uncracked rotor rotating at 22 rad/s. The response is obviously harmonic with rotational speed with same amplitudes in vertical and horizontal directions. In case of the uncracked rotor there is no response in the torsional or axial direction due to the absence of any explicit axial or torsional excitation. Under the similar unbalance excitation conditions, Fig. 5 shows response of the cracked rotor with crack depth ratio of $\bar{a} = 0.2$. The cracked rotor exhibits higher harmonic components in the lateral vibration spectrum (Figs. 5e and f) that are well established in the literature. It also shows the presence of harmonics ($1x$, $2x$, $4x$) in the response of axial and torsional vibration; even though no explicit axial or torsional excitation is applied (Figs. 5g and h). The response in these two modes is due to coupling of lateral, torsional and longitudinal directions.

The torsional excitation is now applied to the cracked rotor with depth ratio of $\bar{a} = 0.2$ rotating at 22 rad/s. The torsional excitation $T_e = M_t \sin(221t)$ at frequency of 221 rad/s is applied for a very short duration of 0.02857 s (equal to period of one cycle). The frequency 221 rad/s is the natural frequency of bending vibrations of the rotor. The exact timing of the application of transient torsional excitation during rotation of the cracked rotor can be varied. Fig. 6 shows the response of the cracked rotor ($\bar{a} = 0.2$) when the transient torsional excitation is applied when rotor is oriented at $\varphi = 0^\circ$.

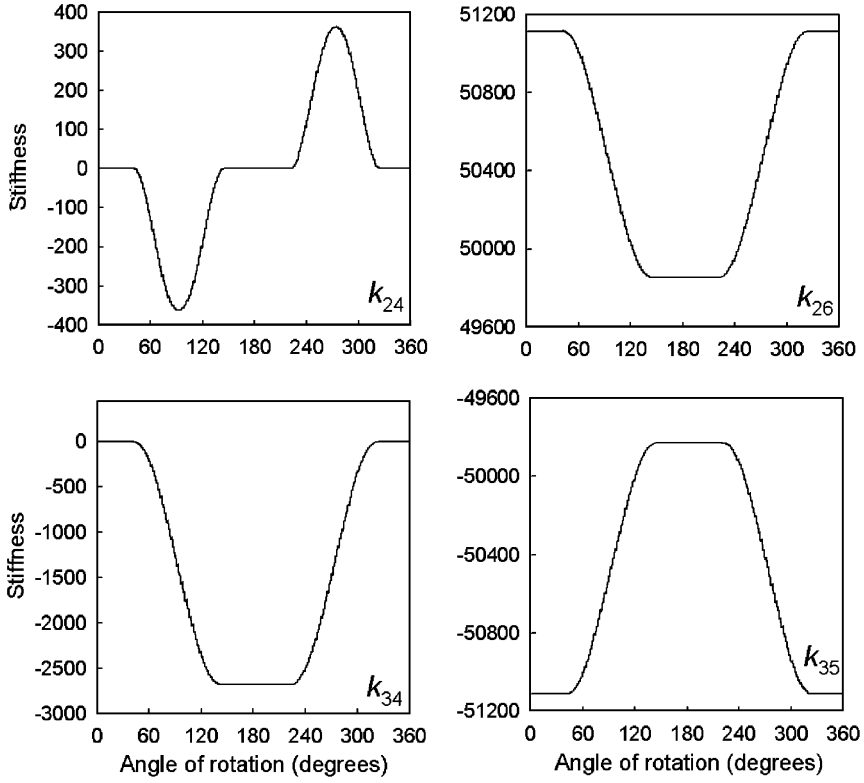

Fig. 3. Variation of cross-coupled stiffness coefficients ($\bar{a} = 0.2$).

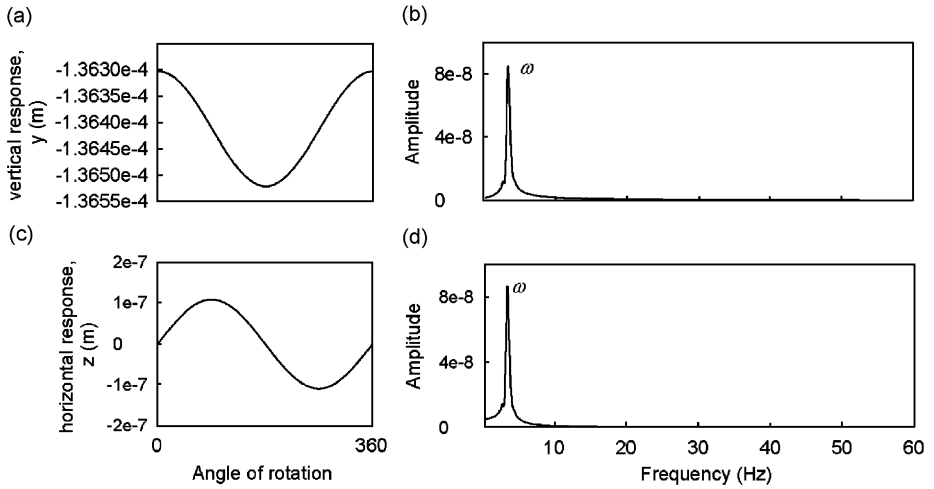

Fig. 4. Unbalance response of an uncracked rotor ($\omega = 22$ rad/s).

The transient torsional excitation is evident from the torsional vibration signal in Fig. 6d at the start of 5th rotation ($\varphi_c = 1440^\circ$). The torsional excitation causes a broadband excitation as seen in the spectrum of the torsional vibration signal (Fig. 6h). Although a transient torsional excitation was applied, the time domain signal in bending and longitudinal vibrations (Figs. 6a–c) do not show any sign of transient disturbance to the rotor after $\varphi_c = 1440^\circ$. It may be mentioned that the excitation is applied when $\varphi = 0^\circ$ (angle turned during the 5th cycle of rotation) and when cumulative angle turned by the rotor from the start is $\varphi_c = 1440^\circ$.

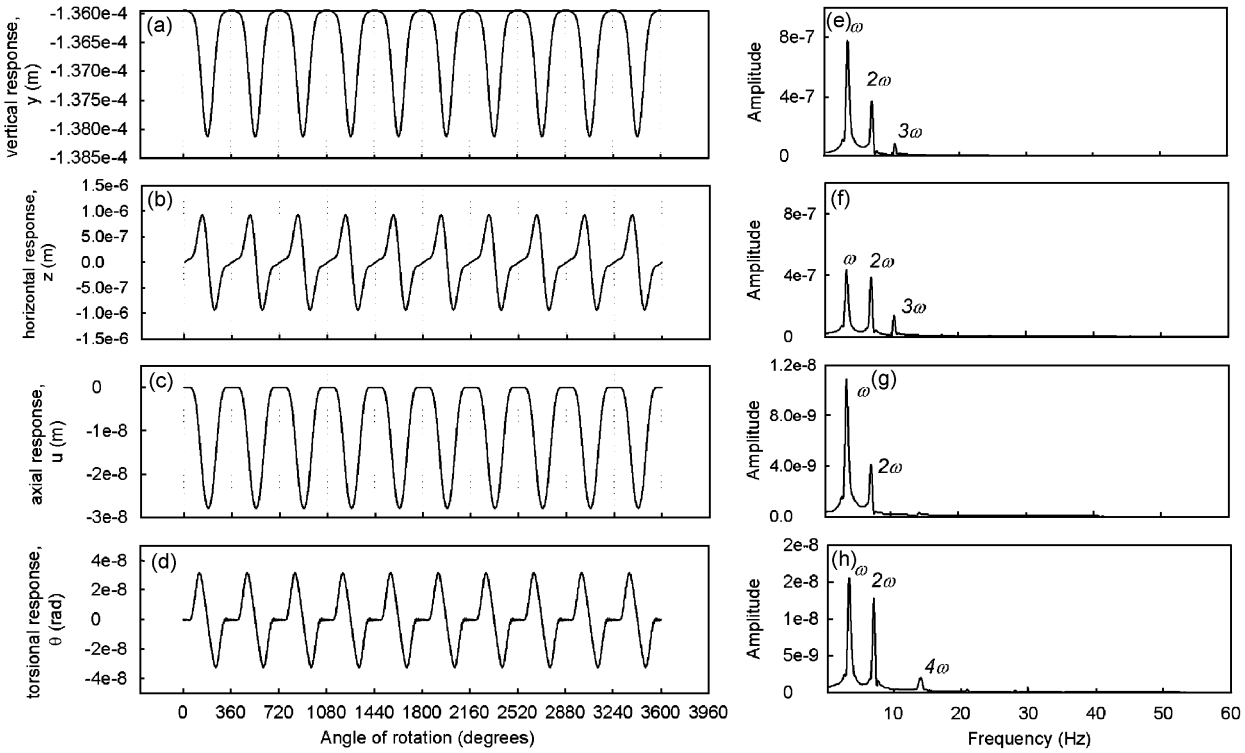

Fig. 5. Unbalance response of a cracked rotor ($\bar{a} = 0.2$) without torsional excitation; $\omega = 22$ rad/s.

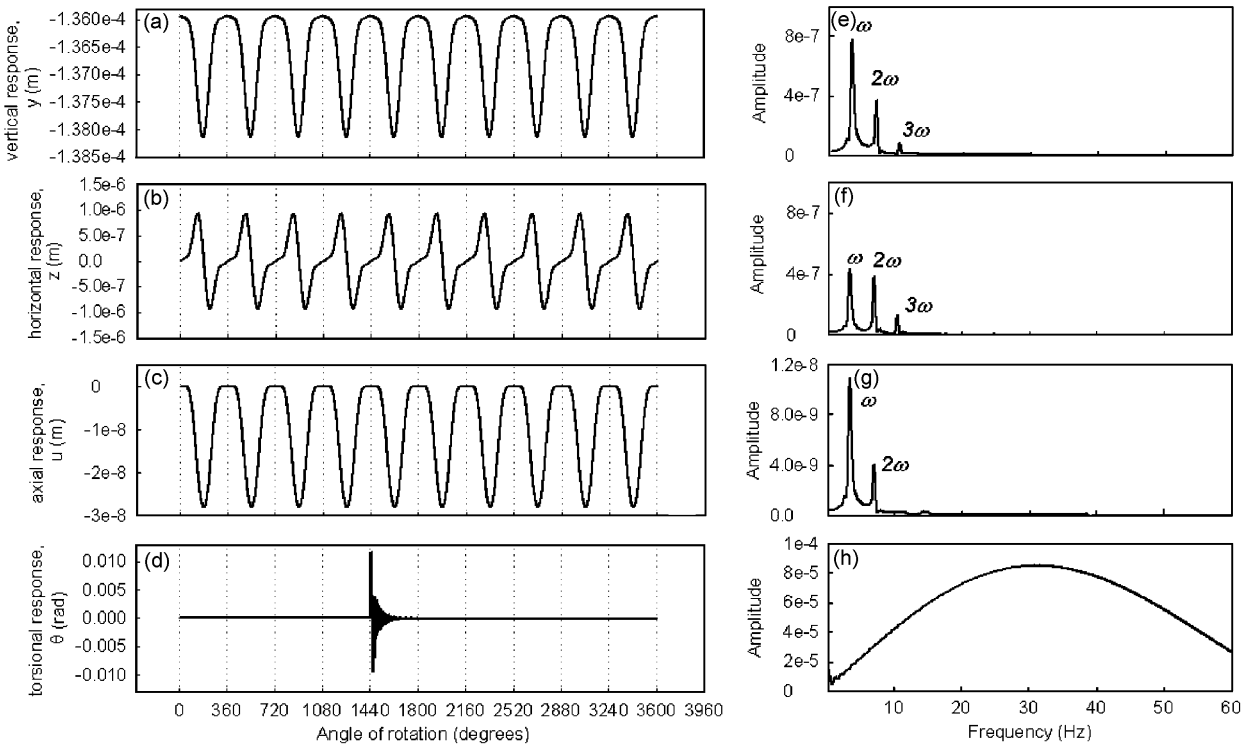

Fig. 6. Unbalance response of a cracked rotor ($\bar{a} = 0.2$) with transient torsional excitation applied at $\varphi = 0^\circ$ during 5th revolution $\omega = 22$ rad/s.

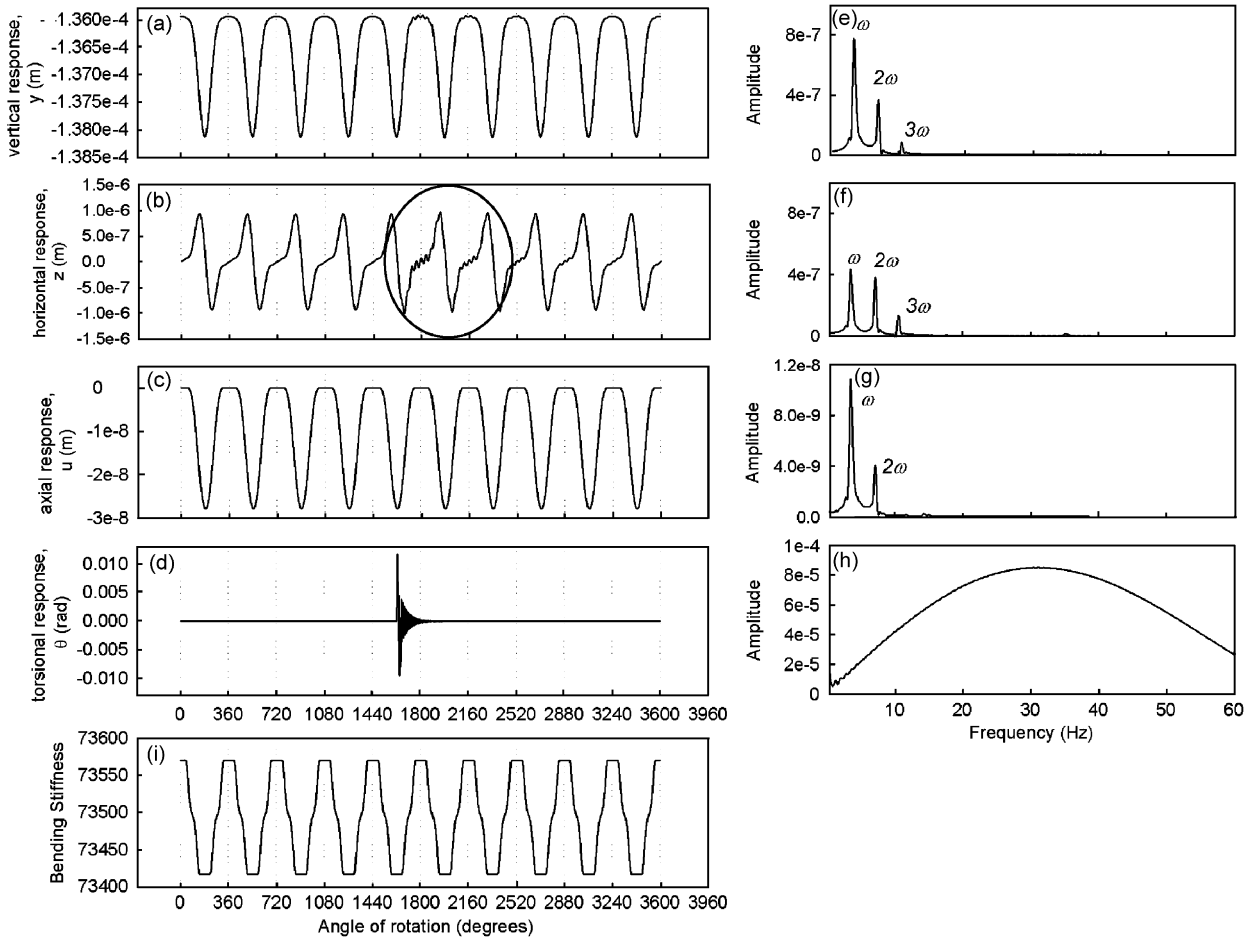

Fig. 7. Unbalance response of a cracked rotor ($\bar{a} = 0.2$) with transient torsional excitation applied at $\varphi = 180^\circ$ during 5th revolution $\omega = 22$ rad/s.

Fig. 7 shows response of the cracked rotor when the same transient torsional excitation is applied at $\varphi = 180^\circ$ during the 5th rotation (i.e., $\varphi_c = 1620^\circ$). In this case, Figs. 7a and b show some noticeable changes in the response for a very short duration for a couple of cycles or rotation ($\varphi_c = 1620$–2520°) after the application of excitation. The changes in the form of high-frequency ripples are more perceptible in horizontal vibrations. However, being for a very short duration, these vibrations are not properly represented in the frequency domain signal of the vibrations shown in Figs. 7e and f. The spectra in Figs. 7e and f are almost identical to those in Figs. 6e and f although the time domain signals are slightly different as the disturbance is noticed in Figs. 7a and b.

When the torsional excitation is applied at the two different angular orientation of the rotor, Figs. 6 and 7 show that there is small and barely noticeable change in time domain signal. There is no change in the longitudinal vibration response in either case. When the excitation is applied at $\varphi = 180^\circ$, the crack is on the underside (in the tensile region) and hence is fully open. A fully open crack allows cross coupling between torsional and bending vibration and torsional excitation generates resonant bending vibrations that dies out quickly and are not sustained beyond couple of cycles of rotation. In contrast, when the torsional excitation applied at $\varphi = 0^\circ$, the crack is at the top side (in the compressive region) and hence is fully closed. In this case the closed crack prevents cross coupling of torsional and bending vibrations; the transient torsional excitation therefore fails to generate any additional response in the bending vibrations. It is also noticed from the bending stiffness variation of the cracked rotor (Fig. 7i) that the application of excitation does not alter the

periodic variation of the stiffness indicating an unchanged opening and closing (breathing) of the crack. The observation is important as it ensures that a different quality of rotor response is generated depending upon whether the excitation is applied at $\varphi = 0^\circ$ (crack closed) or at $\varphi = 180^\circ$ (crack open).

Although a qualitatively different lateral vibration response is observed from Figs. 6a, b and 7a, b, the response dies down quickly causing detection of such transient phenomenon a difficult task using traditional signal analysis techniques such as frequency domain analysis (as evident from Figs. 7e and 7f). WTs are better suited for such situations as they have time localization feature. Wavelet analysis provides an excellent access to information that may be obscured by other techniques.

Over the past 15 years, WTs have become one of the fast-emerging and effective mathematical and signal processing tools for its distinct advantage in analysing signals, particularly the transient ones. Using different window functions through dilation and translation of a prototype function called mother wavelet, the WT can provide multi-resolution (multi-scale) analysis of a signal. Hence it can extract time–frequency features of a signal effectively, which are obscured in the traditional Fourier Transform analysis. The limitation of Fourier Transform stem from the fact that the integral transform is applied on the signal globally and hence in the process time localization of the spectral component is not highlighted and is lost if the transient decays quickly.

To reveal the subtle but important information hidden in the transient vibration signal generated due to transient torsional excitation, the response estimated using a nonlinear rotor dynamic analysis of the cracked rotor is analysed using wavelet analysis. For vibration-based fault diagnosis, usually continuous WTs are employed as the resolution is higher compared to the dyadic type of WT. A continuous type of wavelet transform (CWT) that is applied to the signal $f(t)$ can be defined as [28]

$$C(a,b) = \frac{1}{\sqrt{a}} \int_{-\infty}^{\infty} f(t)\psi\left(\frac{t-b}{a}\right) \mathrm{d}t, \tag{8}$$

where a is the dilation factor (scale), b is the translation factor and $\psi(t)$ is the mother wavelet. $1/\sqrt{a}$ is an energy normalization term.

$C(a,b)$ are refered to as wavelet coefficients which are obviously functions of dilation factor (a) and translation factor (b) for a given mother wavelet. A typical 2D wavelet plot shows absolute values of these coefficients as a function of the dilation and translation parameters. In the scalogram, the x-axis denotes the time parameter whereas the y-axis indicates the scale that is having a reciprocal relationship with the frequency. The colour intensity in the plot of these two parameters (in case of 2D scalogram) is proportional to $|C_{a,b}|^2$, the absolute value of the wavelet coefficient, where as in case of the 3D wavelet scalogram, the height along the z-axis is indicative of the absolute value of these coefficients. The scalogram indicates how energy in the signal is distributed in the time–frequency plane. The wavelet 2D or 3D plot shown subsequently in this section has scale (a) which is inversely related to the frequency value. A low scale value indicates a high frequency, whereas the large scale is indicative of the low frequency [28]. Matlab's (version 7) standard functions are used in the analysis with Morlet mother wavelet. The Morlet wavelet is an exponentially sinusoidal signal and the damped sinusoidal is the common response of many dynamical systems [29]. This wavelet has a single frequency and constructed by modulating a sinusoidal function by a Gaussian function. As mentioned earlier, scale is inversely related the frequency. Though there is no exact mathematical relation for this, with approximation we may write [30]

$$F_a = F_c/(\Delta s), \tag{9}$$

where F_a is the pseudo-frequency (for the scale value s), s the scale, F_c the central frequency of mother wavelet in Hz and Δ the sampling period. Central frequency of the Morlet wavelet is 0.8125 Hz. For most simulations in this study the sampling period is 7.933e−4 s.

Fig. 8 shows the 3D and 2D wavelet scalogram of torsional vibration signal applied at $\varphi = 180^\circ$ ($\varphi_c = 1620^\circ$). It may be observed that the application of excitation is observed in the form of large wavelet coefficient value after $\varphi_c = 1620^\circ$ for a short duration thereafter. The large wavelet coefficients are observed for a wide scale range (from scale value of 4–100 and beyond) indicating that wide band of frequencies are excited at $\varphi_c = 1620^\circ$.

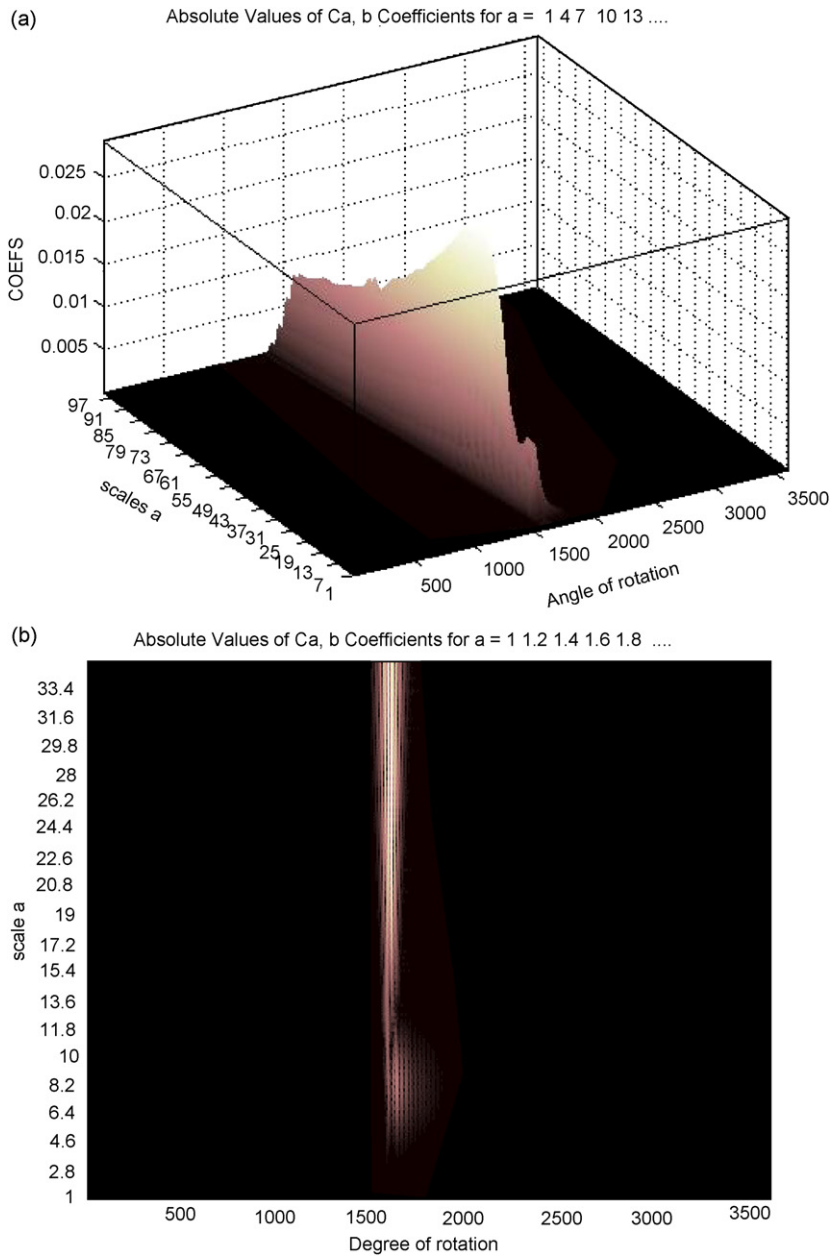

Fig. 8. Wavelet scalogram of the torsional vibration signal with excitation applied at $\varphi_c = 1620^\circ$, i.e., $\varphi = 180^\circ$ (a) 3D, (b) 2D plot.

The broadband torsional excitation also excites the torsional resonance in the torsional vibration signal as observed in Fig. 8b. The scale value of 8.2 maps to the frequency of 125 Hz, which is the torsional natural frequency of the rotor. At the scale value of 8.2 and $\varphi_c = 1620^\circ$, a gradually decreasing coefficient value is observed from the fading white patch between $\varphi_c = 1620^\circ$ and 1900°. This indicates a decaying torsional vibration signal of torsional natural frequency.

The 3D scalogram of lateral vibration signal is shown in Fig. 9a. The x-axis represents the cumulative angle turned by the rotor (φ_c), the y-axis represents the scale value and the z-axis represents the absolute values of wavelet coefficients. The figure represents the wavelet scalogram of the time domain signal of lateral vibration shown in Fig. 7b; wherein the excitation is applied at $\varphi = 180^\circ$. The high-energy concentration is observed at scale values of 293 and 146, which represents $1x$ and $2x$ harmonic frequency components for the rotational

speed of 3.5 Hz. The figure also shows a gradually decreasing ridge (shown encircled) from angle of rotation $\varphi_c = 1620^\circ$ at the scale value of 29 that corresponds to the bending natural frequency (35 Hz) of the cracked rotor. The same 3D plot for the scale value from 1 to 100 is shown in Fig. 9b, that clearly shows the bending natural frequency vibration initiated during the 5th cycle of rotation after the application of excitation at $\varphi_c = 1620^\circ$.

As the scale value of interest is 29, the 2D wavelet map with reduced scale range (Fig. 9c) shows the generation of bending resonance vibration initiated after $\varphi_c = 1620^\circ$ and gradually decays. It may also be observed that although the resonant bending vibrations are seen immediately following the application of torsional excitation at $\varphi_c = 1620^\circ$, the peak value of wavelet coefficient is observed at $\varphi_c = 1693^\circ$ (indicated by

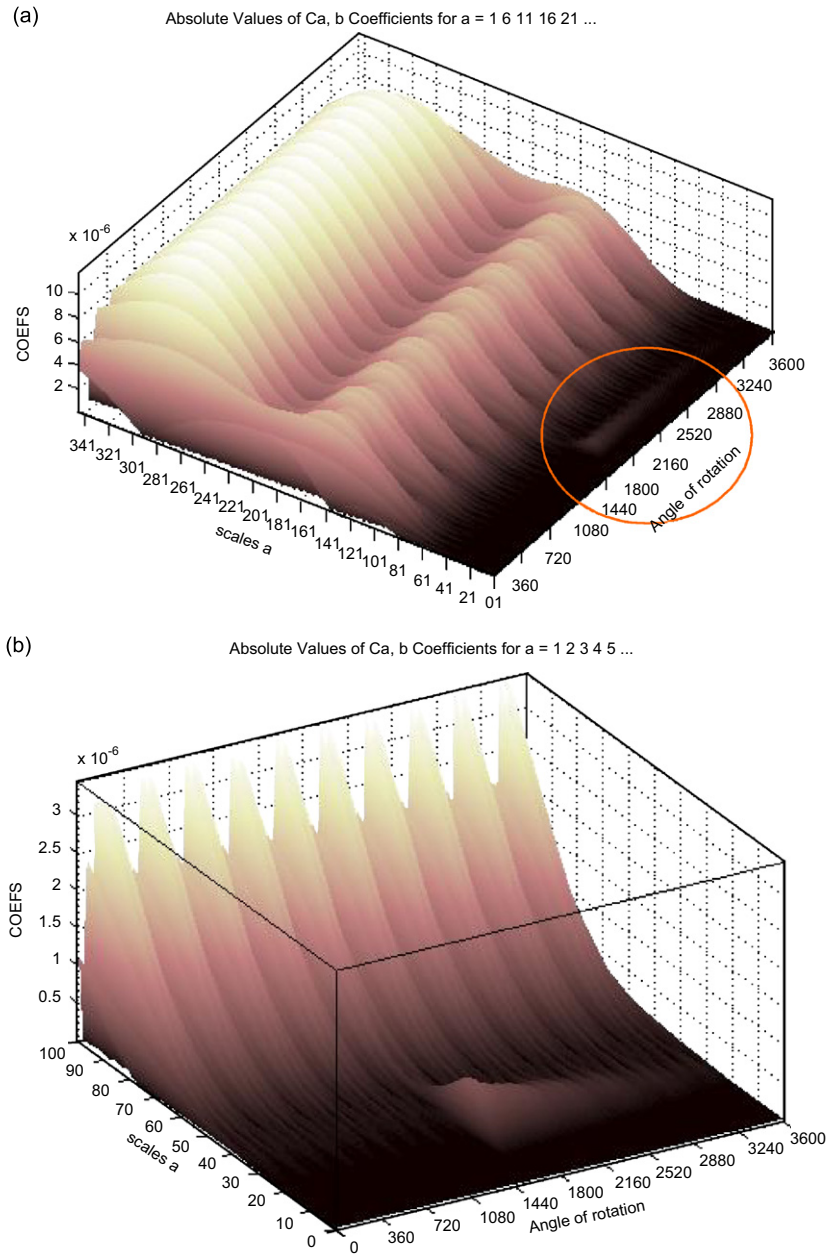

Fig. 9. Wavelet scalogram of the bending vibration signal with excitation applied at $\varphi_c = 1620^\circ$, i.e., $\varphi = 180^\circ$ (a) scale range 1–350, (b) scale range 1–100, (c) 3D scalogram; scale range 1–40, (d) 2D scalogram; scale range 1–40.

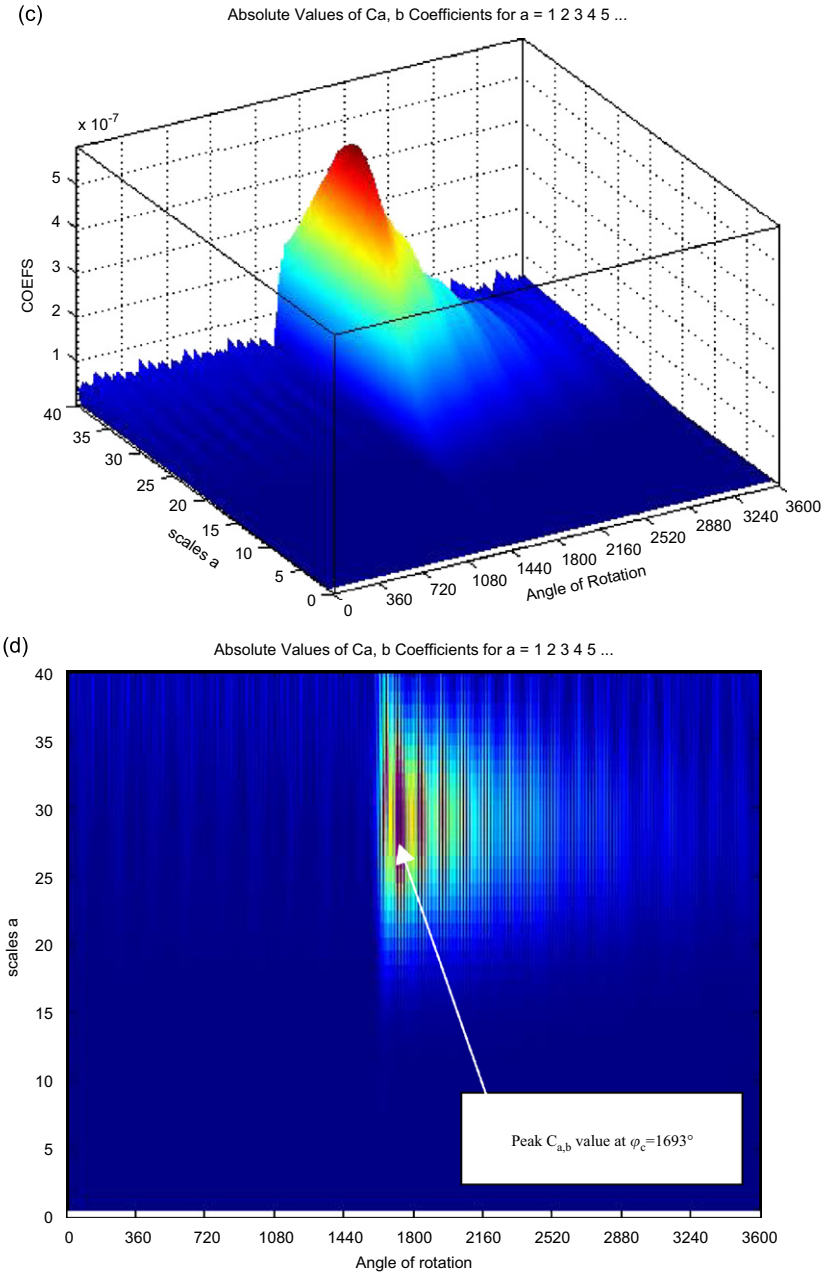

Fig. 9. (*Continued*)

dark brown patch) as it takes finite time to build up resonant vibration. The vibrations decay after $\varphi_c = 1693^\circ$ as seen in Fig. 9d. The excitation is applied in torsional mode and resonant vibrations are observed in the bending mode, indicating coupling of vibrations.

WT is now applied to the bending vibration signal shown in Fig. 6b. All other conditions being the same, only timing of the excitation is different in this case. Instead of applying at $\varphi = 180^\circ$ ($\varphi_c = 1620^\circ$), the excitation is applied at $\varphi = 0^\circ$ ($\varphi_c = 1440^\circ$) when the crack is closed as observed from the stiffness variation in Fig. 7i. Compared to Figs. 9b and d, Figs. 10a and b shows a complete absence of the ridge representing transient resonant bending vibrations at scale value of 29 beyond $\varphi_c = 1440^\circ$. The wavelet map thus can pick

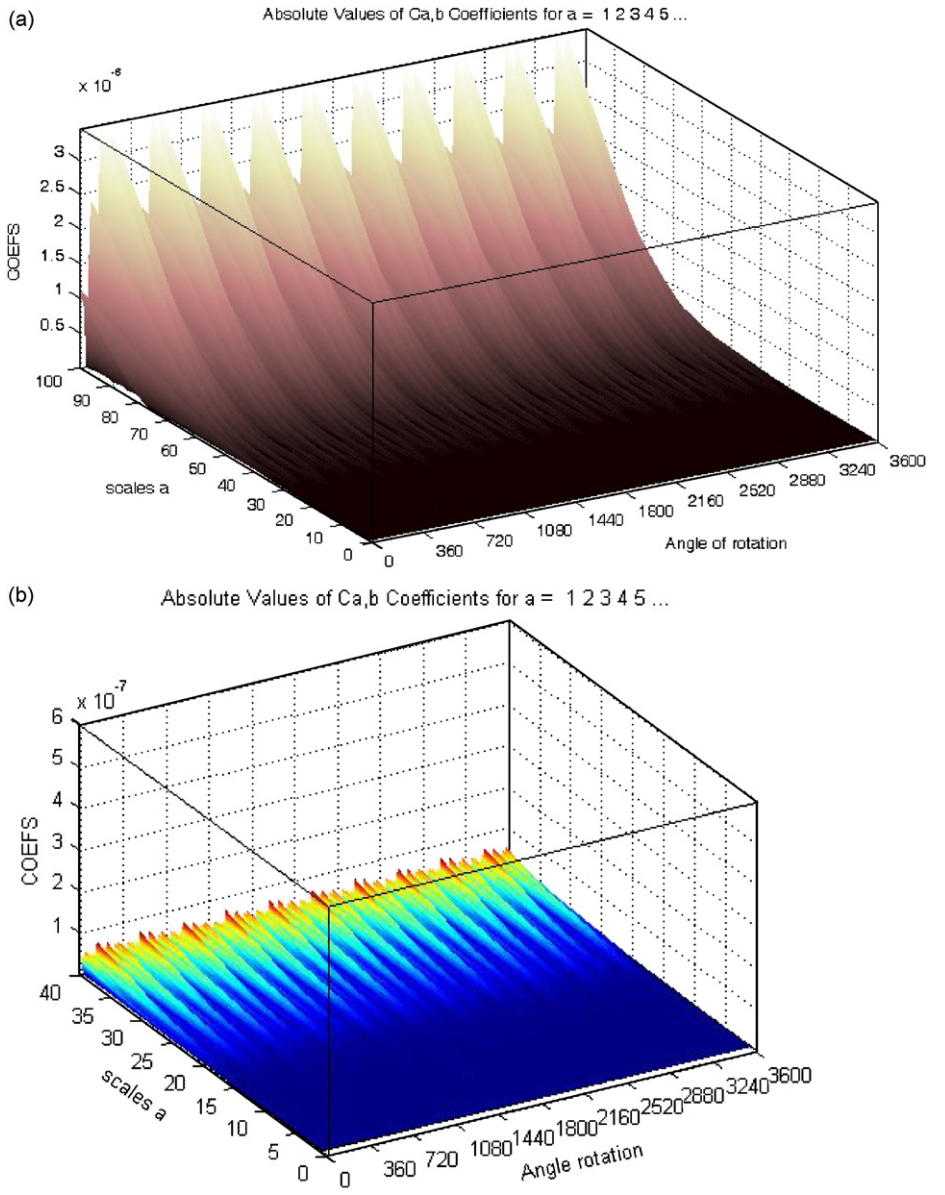

Fig. 10. Wavelet scalogram of the bending vibration signal with excitation applied at $\varphi_c = 1440^\circ$, i.e., $\varphi = 0^\circ$ (a) 3D scalogram; scale range 1–100, (b) 3D scalogram; scale range 1–40.

up the transient part of the signal and locate the presence of these transients in a time–frequency representation shown in Figs. 8 and 9. The exact timing of excitation and the frequency of the transient disturbance can be judged easily from a single graph.

The crack opens and closes gradually and from Fig. 7i it is also clear that the crack remains closed and remains open for a considerable period of time during a rotation. It is important to understand the effect of applying excitation at other orientation of the cracked rotor instead of at $\varphi = 0^\circ$ or at $\varphi = 180^\circ$. $C^p_{a,b}$, the largest value of the $C_{a,b}$ coefficient (hereafter called Peak absolute value of wavelet coefficient) for the scale range of 1–40 and angle of rotation of 0–3600° are estimated for different angular position of cracked rotor (φ) at which torsional excitation is applied. Fig. 11 shows how the coefficient value varies with angular position of excitation for horizontal and vertical vibration signal. As also noted from Figs. 9 and 10, Fig. 11 shows that there is a large difference between the peak absolute coefficient values $C^p_{a,b}$ corresponding to $\varphi = 0^\circ$

or at $\varphi = 180^\circ$. At other values on either side of $\varphi = 180^\circ$, the $C^p_{a,b}$ drops as the excitation is applied in rotor orientations where the crack is partially open and partially closed; the condition leads to a changed value of cross coupled stiffness and changed cross coupling effects.

As mentioned earlier (Fig. 2), the crack starts opening at 40° and opens completely at 140°. It remains open till 220° and then gradually starts closing from 220° till it closes completely at 320°. Thus, any excitation applied between $\varphi = 320^\circ$ and $\varphi = 360^\circ$ and from $\varphi = 0^\circ$ to $\varphi = 40^\circ$ is not expected to give rise to a high value of coefficient which is revealed from Fig. 11. For the case of excitation applied at $\varphi = 216^\circ$ the coefficient value is less compared to the case of $\varphi = 180^\circ$ although the crack is fully open till $\varphi = 220^\circ$. It may be noted

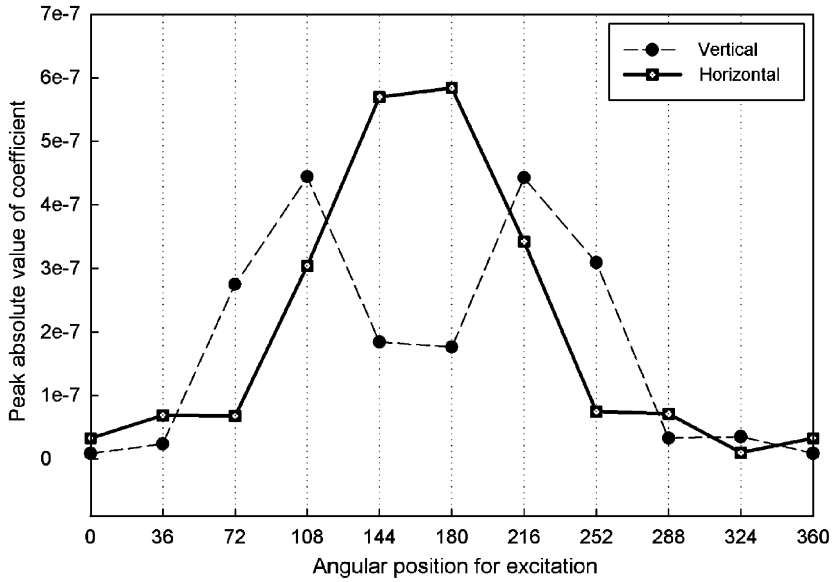

Fig. 11. Variation of peak absolute coefficient $C^p_{a,b}$ corresponding to vertical and horizontal vibration of rotor with angular position of excitation φ.

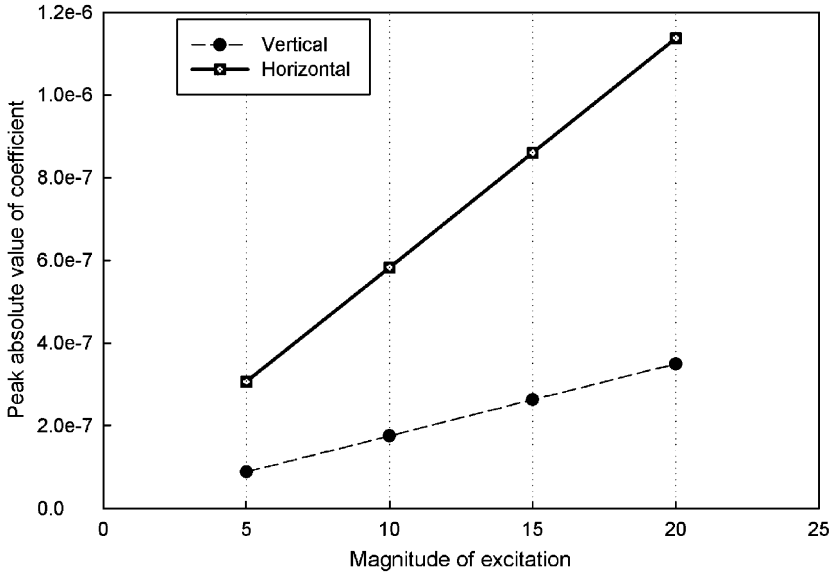

Fig. 12. Sensitivity of $C^p_{a,b}$ to magnitude of excitation M_t.

that it takes some time for the resonance to build up and by that time the crack has already started to close beyond $\varphi = 220^\circ$. The coefficient value variation estimated for the rotor vibration signal in the vertical direction (z) is somewhat different than the one for horizontal direction (y). In this case, if the excitation is applied at the rotor angles at which the crack is partially open/partially closed ($40^\circ < \varphi < 140^\circ$ and $220^\circ < \varphi < 320^\circ$), the peak value of coefficient $C^p_{a,b}$ in vibration in vertical direction is more than the one for horizontal vibration. On the contrary, when the excitation is applied at angles corresponding to the fully open or fully closed crack ($0^\circ < \varphi < 40^\circ$ and $320^\circ < \varphi < 360^\circ$), the peak coefficient value $C^p_{a,b}$ is less for vertical

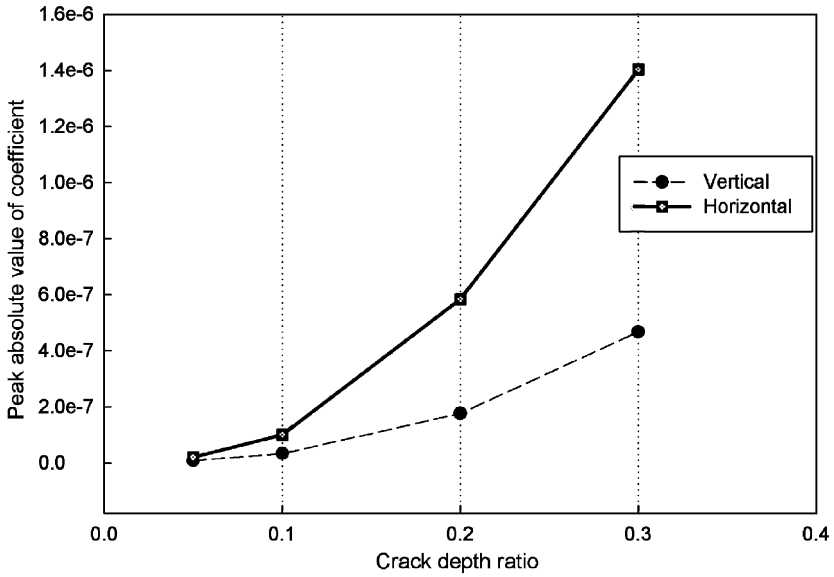

Fig. 13. Sensitivity of $C^p_{a,b}$ to crack depth ratio $\bar{a}$.

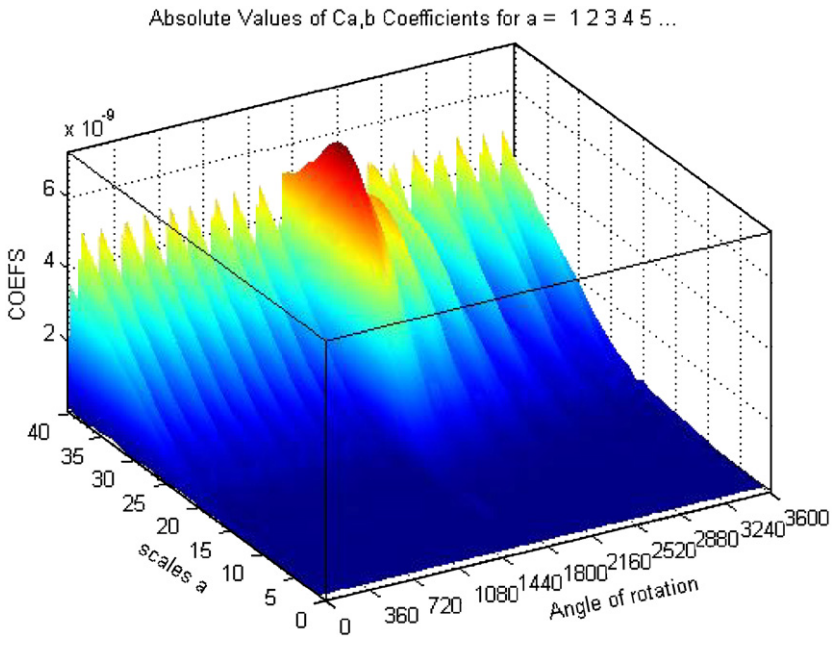

Fig. 14. Wavelet scalogram of the bending vibration signal with excitation applied at $\varphi = 180^\circ$ for shallow crack ($\bar{a} = 0.05$).

vibration than the one for horizontal vibration. These distinctive directional features can also aid in the detection of the presence of crack.

Fig. 12 shows the sensitivity of the $C^p_{a,b}$ to the magnitude of torsional excitation M_t. The value of $C^p_{a,b}$ increases linearly with the magnitude of torsional excitation. The coefficient $C^p_{a,b}$ corresponding to horizontal vibrations is more sensitive to magnitude of torsional excitation compared to that of vertical vibrations.

Fig. 13 shows the sensitivity of the peak absolute value of the wavelet coefficient, $C^p_{a,b}$ to the depth of crack $\bar{a}$. The figure shows that the $C^p_{a,b}$ is highly sensitive to the depth of the crack. The value of $C^p_{a,b}$ estimated for the rotor vibration signal in horizontal direction is much more sensitive than the one for vertical direction. At such lower crack depths of 10% of rotor diameter, the $C^p_{a,b}$ is highly sensitive to change in the crack depth. In fact, even for a crack depth of 5% of rotor diameter ($\bar{a} = 0.05$), the presence of transient bending vibration could be easily observed as shown in Fig. 14. The substantial difference in the horizontal and vertical value of

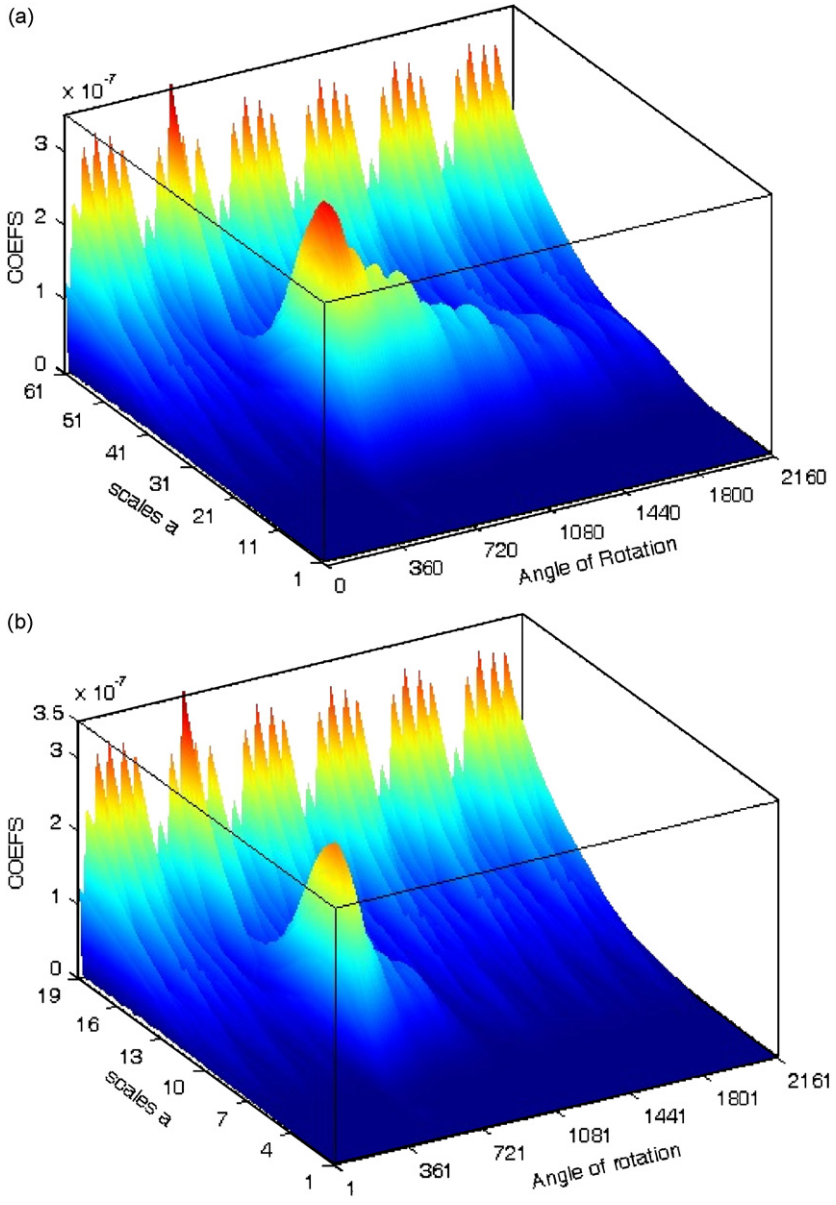

Fig. 15. Wavelet scalogram of the bending vibration signal with excitation applied at $\varphi = 180^\circ$ ($\bar{a} = 0.2$) for different levels of damping; (a) modal damping ratios of 0.005 and 0.01, (b) modal damping ratios of 0.05 and 0.08.

$C^{p}_{a,b}$, at all the crack depths can also be used as additional information for crack detection; although the very presence of transient resonant bending vibration due to transient torsional excitation is a strong indicator of the presence of a crack. The presence or absence of such resonant bending vibration depending upon whether angular position of excitation can be expected only for the crack as it is directly linked to the breathing of crack. Most other faults do not exhibit this kind of behaviour. The use of WT makes it easier to detect the transient nature of bending vibration and allows the user to apply torsional excitation at various angular orientation to exploit the crack breathing for crack detection. The detection methodology discussed here also avoids use of sustained application of external torsional excitation and only very short duration excitation is required.

The effect of damping on the observed response is investigated for different levels of damping. Analysis with change in the modal damping ratio value within a reasonable range (by increasing the first two modal damping ratios from 0.005 and 0.01 to 0.01 and 0.05, respectively) resulted in no change in the response. Only when the modal damping ratio was increased substantially from 0.005 and 0.01 to 0.05 and 0.08 (i.e., by about 10 times), that some perceptible changes were observed in the response (Fig. 15). Even in this case, it may be noted that the level damping does not significantly change the level of peak coefficient observed after the application of transient torsional excitation. The peak coefficient drops from 3.22e−7 to 2.73e−7 when the damping is increased by about 10 times as mentioned above.

The large increase in the damping level in the system has only influenced the damped exponential decay in the transient response as observed from Fig. 15. However, even such a large change in the value of damping does not alter the presence of transient vibration set-up in the system which is solely related to the presence of coupling phenomenon (between torsional and lateral vibrations) for the cracked rotor. The use of WT for detecting this coupling phenomenon owing to the presence of crack through identification of transient vibration response exploits the very basic feature of WT in localizing the feature in time.

4. Conclusions

A novel way to detect fatigue transverse cracks in rotors is presented. A detection methodology is formulated that truly exploits the breathing phenomenon of the crack for its diagnosis. The coupling of bending and torsional vibrations is the basis for the proposed methodology in general and the presence/absence of such cross coupling terms at various orientation of crack in a rotor due to its opening and closing under the influence of gravity, in particular. A transient torsional excitation is applied for a very short duration at specific angular orientation of the rotor and its effect in the lateral vibrations is investigated. WTs is used in revealing the transient features of the resonant bending vibrations, which are set up for a short duration of time upon transient torsional excitation. The peak absolute value of wavelet coefficient is significantly different depending upon whether the excitation is applied when the crack is open or when it is closed. A typical variation of peak absolute coefficient value with angle at which excitation is applied is obtained that is in conformity with the breathing pattern of the crack. The nonlinear breathing crack model is used in the study that helps in understanding the exact breathing phenomenon. It also helps in utilizing the breathing for timing the excitation and interpretation of results.

The sensitivity analysis is performed that shows that the peak absolute value of wavelet coefficient is highly sensitive to the depth of crack and even a very shallow crack (5% of rotor diameter) can be detected. The value of this coefficient for bending vibration in horizontal direction is highly sensitive to depth of crack and hence can be used for early detection of crack in rotors. There is a distinct difference between the value of the coefficient corresponding to the rotor response in horizontal and vertical directions, which can be used as addition information for the crack diagnosis based on the proposed methodology. The use of breathing phenomenon of crack, its subsequent effect on coupling of vibrations, capturing the transient response in lateral vibrations due to transient torsional excitation using WT and using this presence or absence of transient response by applying excitation at different angular orientation of crack during rotation is indeed a novel approach to diagnose the crack. The fact that the rotor is not required to stop and the detection process is applied for a rotating shaft makes the methodology more versatile, convenient and unambiguous.

References

[1] J. Schmied, E. Kramer, *Vibrational behaviour of a rotor with a cross-sectional crack, Vibrations in Rotating Machinery*, Institution of Mechanical Engineers Publications, London, 1984, pp. 183–192.

[2] W. Mayes, W.G.R. Davies, Analysis of the response of the multi-rotor-bearing system containing a transverse crack in a rotor, *Journal of Vibration, Acoustics, Stress and Reliability in Design* 106 (1984) 139–145.

[3] N. Bachschmid, G. Diana, B. Pizzigoni, *The influence of unbalance on cracked rotors. Vibrations in Rotating Machinery*, Institution of Mechanical Engineers Publications, London, 1984, pp. 193–198.

[4] B. Grabowski, The vibrational behaviour of a rotating shaft containing a transverse crack, in: O. Mahrenholtz (Ed.), *Dynamics of Rotors & Stability and System Identification. CISM Courses & Lectures*, Vol. 273, Springer, New York, 1984, pp. 423–465.

[5] Imam, S.H. Azzaro, R.J. Bankert, J. Scheibel, Development of an on-line rotor crack detection and monitoring system, *Journal of Vibration, Acoustics, Stress and Reliability in Design* 111 (1989) 241–250.

[6] O.S. Jun, H.J. Eun, Y.Y. Earmme, C.W. Lee, Modelling and vibration analysis of a simple rotor with a breathing crack, *Journal of Sound and Vibration* 155 (1992) 273–290.

[7] M.C. Wu, S.C. Huang, In-plane vibration and crack detection of a rotating shaft-disk containing a transverse crack, *Journal of Vibration and Acoustics* 120 (1998) 551–556.

[8] C.A. Papadopoulos, A.D. Dimarogonas, Coupled longitudinal and bending vibrations of a rotating shaft with an open crack, *Journal of Sound and Vibration* 117 (1987) 81–93.

[9] C.A. Papadopoulos, A.D. Dimarogonas, Coupling of bending and torsional vibration of a cracked Timoshenko shaft, *Ingenieur-Archiv* 57 (1987) 257–266.

[10] A. Muszynska, P. Goldman, D.E. Bently, Torsional/lateral vibration cross-coupled responses due to shaft anisotropy: a new tool in shaft crack detection, *Vibrations in Rotating Machinery*, Institution of Mechanical Engineers Conference Publications, London, 1992, pp. 257–262.

[11] W.M. Ostachowicz, M. Krawczuk, Coupled torsional and bending vibrations of a rotor with an open crack, *Archives of Applied Mechanics* 62 (1992) 191–201.

[12] A. Papadopoulos, A.D. Dimarogonas, Coupled vibration of cracked shafts, *Journal of Vibration and Acoustics* 114 (1992) 461–467.

[13] C.A. Papadopoulos, A.D. Dimarogonas, Stability of cracked rotors in the coupled vibration mode, *Journal of Vibration, Acoustics, Stress and Reliability in Design* 110 (1988) 356–359.

[14] A.K. Darpe, A. Chawla, K. Gupta, Analysis of the response of a cracked Jeffcott rotor to axial excitation, *Journal of Sound and Vibration* 249 (2002) 429–445.

[15] A.K. Darpe, K. Gupta, A. Chawla, Experimental investigations of the response of a cracked rotor to axial excitation, *Journal of Sound and Vibration* 260 (2003) 265–286.

[16] K.R. Collins, R.H. Plaut, J. Wauer, Detection of cracks in rotating Timoshenko shafts using axial impulses, *Journal of Vibration and Acoustics* 113 (1991) 74–78.

[17] G.D. Gounaris, C.A. Papadopoulos, Crack identification in rotating shafts by coupled response measurements, *Engineering Fracture Mechanics* 69 (2002) 339–352.

[18] A.K. Darpe, K. Gupta, A. Chawla, Coupled bending, longitudinal and torsional vibrations of a cracked rotor, *Journal of Sound and Vibration* 269 (2004) 33–60.

[19] J.-J. Sinou, A.W. Lees, The influence of cracks in rotating shafts, *Journal of Sound and Vibration* 285 (2005) 1015–1037.

[20] A.S. Sekhar, Crack identification in a rotor system: a model-based approach, *Journal of Sound and Vibration* 270 (2004) 887–902.

[21] P. Pennacchi, N. Bachschmid, A. Vania, A model-based identification method of transverse cracks in rotating shafts suitable for industrial machines, *Mechanical Systems and Signal Processing* 20 (2006) 2112–2147.

[22] S.A. Adewusi, B.O. Al-Bedoor, Wavelet analysis of vibration signals of an overhang rotor with a propagating transverse crack, *Journal of Sound and Vibration* 246 (2001) 777–793.

[23] J. Zou, J. Chen, Comparative study on time–frequency feature of cracked rotor by Wigner–Ville distribution and wavelet transform, *Journal of Sound and Vibration* 276 (2004) 1–11.

[24] F. Wan, Q. Xu, S. Li, Vibration analysis of cracked rotor sliding bearing system with rotor–stator rubbing by harmonic wavelet transform, *Journal of Sound and Vibration* 271 (2004) 507–518.

[25] J. Zou, J. Chen, Y.P. Pu, Wavelet time-frequency analysis of torsional vibrations in rotor system with a transverse crack, *Computers & Structures* 82 (2004) 1181–1187.

[26] S. Prabhakar, A.S. Sekhar, A.R. Mohanty, Detection and monitoring of crack in a coast-down rotor supported on fluid film bearings, *Mechanical Systems and Signal Processing* 15 (2001) 447–450.

[27] H.D. Nelson, A finite rotating shaft element using Timoshenko Beam Theory, *Journal of Mechanical Design* 102 (1980) 793–803.

[28] R.M. Rao, A.S. Bopardikar, *Wavelet Transforms: Introduction to Theory and Applications*, Pearson Education Asia, Delhi, India, 1998.

[29] Z. Peng, Y. He, Q. Lu, F. Chu, Feature extraction of the rub-impact rotor system by means of wavelet analysis, *Journal of Sound and Vibration* 259 (2003) 1000–1010.

[30] M. Misiti, Y. Misiti, G. Oppenheim, J.M. Poggi, *Wavelet Toolbox for Use with Matlab, User's Guide (Version 3)*, The Mathworks Inc., MA, USA, 2006.